# Human-Aware Object Placement for Visual Environment Reconstruction

Hongwei Yi[1] Chun-Hao P. Huang[1] Dimitrios Tzionas[1] Muhammed Kocabas[1,2]
Mohamed Hassan[1] Siyu Tang[2] Justus Thies[1] Michael J. Black[1]
[1]Max Planck Institute for Intelligent Systems, Tübingen, Germany [2] ETH Zürich
{firstname.lastname}@{tuebingen.mpg.de,inf.ethz.ch}

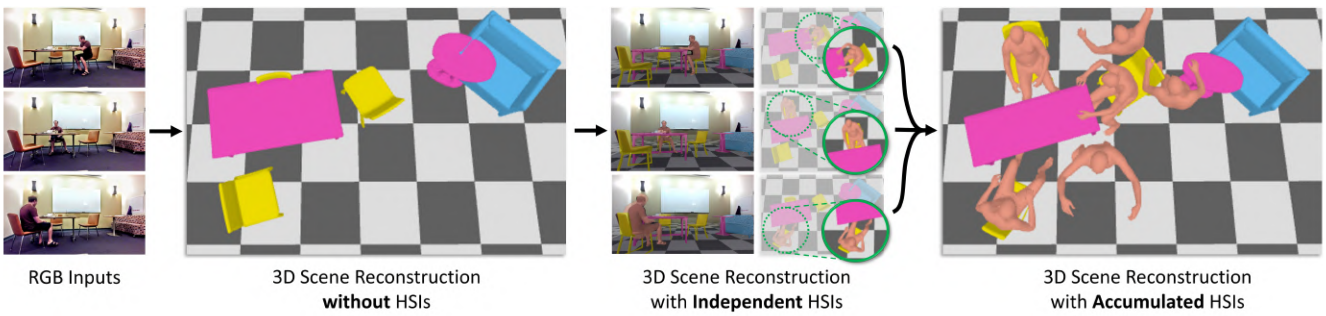


Figure 1. From a monocular video sequence, MOVER reconstructs a 3D scene that best affords humans interacting with it. Existing methods for monocular 3D scene reconstruction ignore people and produce physically implausible scenes. MOVER takes as input: (1) several images of human-scene interaction (HSI) from a static camera, (2) a rough estimate of 3D object shape and placement in 3D space [64], and (3) estimated 3D human bodies interacting with the scene [45, 66]. Each frame contains valuable information about humans, objects, and the proximal relationship between them. MOVER accumulates this information across frames, to optimize for a physically plausible 3D scene. The final 3D scene is more accurate than the input and enables reasoning about human-scene contact.

## Abstract

*Humans are in constant contact with the world as they move through it and interact with it. This contact is a vital source of information for understanding 3D humans, 3D scenes, and the interactions between them. In fact, we demonstrate that these human-scene interactions (HSIs) can be leveraged to improve the 3D reconstruction of a scene from a monocular RGB video. Our key idea is that, as a person moves through a scene and interacts with it, we accumulate HSIs across multiple input images, and use these in optimizing the 3D scene to reconstruct a consistent, physically plausible, 3D scene layout. Our optimization-based approach exploits three types of HSI constraints: (1) humans who move in a scene are occluded by, or occlude, objects, thus constraining the depth ordering of the objects, (2) humans move through free space and do not interpenetrate objects, (3) when humans and objects are in contact, the contact surfaces occupy the same place in space. Using these constraints in an optimization formulation across all observations, we significantly improve 3D scene layout reconstruction. Furthermore, we show that our scene reconstruction can be used to refine the initial 3D human pose and shape (HPS) estimation. We evaluate the 3D scene layout reconstruction and HPS estimates qualitatively and quantitatively using the PROX and PiGraphs datasets. The code and data are available for research purposes at https://mover.is.tue.mpg.de.*

## 1. Introduction

Human behavior and the interaction of humans with their environment are fundamentally about the 3D world. Hence, 3D reconstruction of both the human and scene can facilitate behavior analysis. Where and how humans interact with a scene can be used to predict future motions and interactions for human-centered AI and robots, or to synthesize these for AR/VR and other computer-graphics applications.

Tremendous progress has been made in reconstructing 3D human bodies [12, 37, 39, 44–46, 58, 66, 67, 79, 92, 93] and 3D scenes [6, 17, 31, 64, 95] from monocular images or videos, typically in isolation from each other. In real life, though, humans always interact with scenes. Consequently, humans (partially) occlude the scene, and the scene (partially) occludes humans. Strong human-scene occlusion can cause problems for both scene and human reconstruction.

In contrast, recent work on human-scene interaction (HSI), estimates humans and scenes together [10, 26, 87].

PROX [26] demonstrates how HSI can be used to constrain 3D human pose estimation, but it requires a 3D scan of the full scene to be known a priori. This is often unrealistic and cumbersome, as it requires one to conduct offline 3D reconstruction by walking around the scene with a depth sensor [103] to observe it from many view points.

What we need, instead, is a method that estimates the scene and humans from images of a single color camera. This is challenging, as the lack of depth information causes the scale and placement of objects to be inconsistent w.r.t. the humans interacting with them. This leads to physically implausible results, like humans penetrating objects, or lacking physical contact when walking, sitting, or lying down, causing bodies to "hover" in the air (see Fig. 2). Methods that reconstruct 3D humans from single views leverage statistical body models [38, 56, 66, 90] as priors on the body shape and pose. However, the same tools do not exist for the collective space of 3D scene layouts. This is due to the enormous space of possible object arrangements in indoor 3D scenes, the large number of different object classes, and the huge inter-class (e.g., chairs and desks) and intra-class (e.g., desk chair and club chair) shape variability.

To address the above issues, we present MOVER, which stands for "human Motion driven Object placement for Visual Environment Reconstruction". MOVER leverages information across several HSI frames to estimate both a plausible 3D scene and a moving human that interacts with the scene. Figure 1 provides a high-level overview. MOVER takes as input: (1) a set of color frames from a static monocular camera, (2) a 3D human mesh inferred for each frame [45, 66], and (3) a 3D shape inferred for each object detected in the scene [42, 64]. As output, MOVER produces a refined 3D scene, comprised of repositioned input objects, so that it is consistent with the estimated 3D human; i.e., it satisfies the expected contacts on the body [27], while preventing interpenetration. MOVER uses a novel optimization scheme, that jointly optimizes over camera pose, ground-plane pose, and the size and position of 3D objects, while being constrained by various HSI constraints.

MOVER takes three types of HSI constraints into account: (1) humans who move in a scene are occluded or occlude objects, thus, defining the depth ordering of the objects (c.f. [75]), (2) humans move in free space that is not occupied by objects and do not interpenetrate objects, (3) contact between humans and objects means that the contacting parts of their surfaces occupy the same place in space. Thus, we leverage both explicit (i.e., contact) and implicit (i.e., free space, no penetrations) HSI cues. MOVER is able to use these because it employs detailed meshes for both the scene and the moving human. In contrast, the few attempts that have been made in this direction use oversimplified shapes [10], i.e., 3D bounding boxes for objects and skeletons for humans, work only for static humans that contact

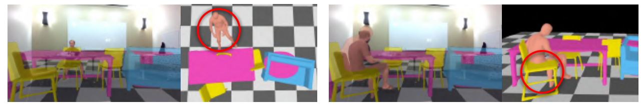

(a) 3D scene reconstruction [64] and HPS [66] in isolation.

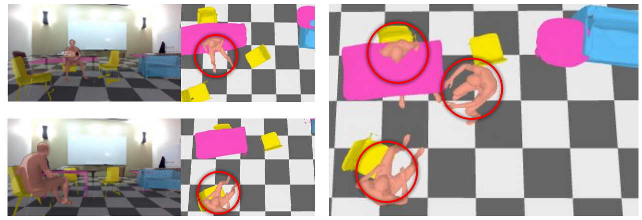

(b) HolisticMesh [87]. L: single-image results. R: multiple-images result.

Figure 2. Where existing methods struggle: (a) humans in estimated scenes penetrate objects or lack contact with objects and "hover" in the air when estimated in isolation [64, 66] (b) humans interpenetrate objects, even, when the 3D scenes and humans are jointly optimized with single (left) or sequential images (right) [87]. In contrast, we leverage human scene interaction constraints in a global optimization across all input frames, to compute a scene that is coherent with the human motions (see Fig. 1).

a single object [96], or do not integrate information across several interaction frames [10, 87, 96].

Comparisons against the state of the art on the PROX [26] and PiGraphs [74] datasets show, that MOVER estimates more accurate and realistic 3D scene layouts that satisfy the expected contacts, while minimizing penetrations, w.r.t. the moving humans. Interestingly, we find that MOVER's estimated 3D scene can be used to refine the human poses, with a PROX-like method [26]. While estimating 3D scenes and humans from a single camera is challenging, our results suggest that they are synergistic tasks that benefit each other.

## 2. Related Work

**Single-view 3D Human Pose in "Isolation":** Estimating human pose from an image is a long standing problem [62, 73]. Typically, this is cast as estimating 2D or 3D joints of body [2, 60, 69, 82, 83] or whole-body skeletons [7, 36, 86]. Recently, there has been a significant shift in research interest towards reconstructing the 3D human body surface which, in contrast to the joints, interacts directly with objects and can be observed by commodity cameras. To this end, many non-parametric methods [21, 47, 71, 72, 78, 84, 89, 102] have been developed, that estimate either depth maps [21, 78], 3D voxels [84, 102], 3D distance fields [71, 72], or free-form 3D meshes [47]. While these methods can reconstruct bodies with details like hair and clothing, they do not encode body parts or provide correspondence across people and poses. In contrast, parametric statistical 3D shape models of the body [3, 25, 56] or body, face, and hands [38, 66, 70, 90] provide this information and allow re-posing. Since parametric models represent the

| Method | GDI | Cam. | C-HOI | N-HOI | FGC |
|---|---|---|---|---|---|
| PHOSA [96] | ✓ | ✗ | ✓ | ✗ | ✗ |
| Holistic++ [10] | ✗ | ✗ | ✗ | ✗ | ✓ |
| HolisticMesh [87] | ✓ | ✓ | ✓ | ✗ | ✓ |
| **Ours** | ✓ | ✓ | ✓ | ✓ | ✓ |

Table 1. Comparison of the most relevant methods. GDI: Geometric Detailed Interaction. C-HOI: Contact-Human-Object Interaction. N-HOI: Exploiting free space constraints with no object contact. FGC: Feet-Ground Contact. Cam.: Camera orientation and ground-plane are refined with humans or not.

shape and pose in a low-dimensional space, they are a powerful tool to estimate the surface from incomplete data (e.g., 2D images with occlusions) through optimization [5, 38, 66, 88], regression [13, 39, 40, 44, 46], or hybrid approaches [37]. However, all the above methods reason about the human in "isolation", i.e. without taking the surrounding objects and scenes into account. Thus, they struggle to reconstruct details like contact with objects, and often fail due to occlusions (e.g., bodies standing behind furniture). PARE [45] addresses this by leveraging localized features and attention, gaining robustness to occlusions. We initialize our approach with [45] to refine the 3D scene layout.

**Single-view 3D Scene in Isolation:** 3D reconstruction from single views has been addressed in several recent works that leverage learned geometric priors for specific object classes or entire scenes. Shapes from single views are reconstructed using generative models for specific object classes [14, 24, 61, 77, 85]. The methods differ in the underlying representation, which ranges from volumetric representations like occupancy fields [61] and implicit surface functions [55, 65], to explicit surface representations like triangular meshes [22, 85]. To reconstruct scenes, single objects can be detected [28] and reconstructed in isolation. Mesh-RCNN [22] detects the objects in an RGB image, and predicts geometry for each object individually. Instead of a generative mesh model, Izadinia et al. [33] and Kuo et al. [48] retrieve individual CAD models for the detected objects in the scene. Bansal et al. [4] infer a normal map from the input image that is used to align a retrieved CAD model. Instead of predicting normal maps from the input image, several methods estimate depth maps [20, 23, 50, 76], or pixel-aligned implicit functions for objects [71, 72, 89] and scenes [17, 19]. Joint estimation of the room layout and objects with scene context information is done for isolated 3D scenes without humans in them [11, 31, 32, 64, 95, 100, 101].

Note that there are also methods that predict room layouts with 3D bounding boxes [18, 29, 51, 59]. In contrast, we reconstruct the detailed object geometry to leverage explicit contact point constraints based on the human scene interactions, while optimizing for the scene layout.

**3D Human-Scene Interaction:** Humans inhabit 3D scenes. Several methods model this and learn to populate a 3D scene [27, 52, 98, 99]. In contrast, our work reasons about the human and its interaction with the 3D scene from RGB observations. There are several methods that explore different kinds of HSI; these can be divided into three categories by the interaction granularity between the human and scene: (1) Hand-Object [8, 9, 34, 49, 54, 81, 91]. (2) Body-Object [16, 43, 53, 80, 96]. (3) Body-Scene [10, 26, 30, 63, 74, 87].

Our proposed method focuses on reconstructing 3D scenes composed of objects and structural elements like the floor plane, using accumulated human scene interactions (body-objects and body-scene). Table 1, overviews the most related work that operates on single-view RGB images/videos. PHOSA [96] infers humans and objects together when they are in contact. They do not consider the fact that humans do not need to contact an object to constrain its location; their movement through free space constrains object placement. Zanfir et al. [94] only consider feet-ground contact. iMapper [63] maps RGB videos to dynamic "interaction snapshots", by learning "scenelets" from PiGraphs data and fitting them to videos. However, the estimated scene is not aligned with the 2D image, and consists of predefined CAD templates with fixed shape and size. Holistic++ [10] takes learned 3D HOI (Human Object Interaction) into account to jointly reason about the arrangement of bodies and objects. Both [63] and [10] do not model geometrically detailed human-scene interaction, due to their simplified representation of the scene and bodies. Weng et al. [87] jointly optimize the reconstructed mesh-based 3D scene and bodies, which are initialized from [64] and [66]. The approach only considers interpenetration between objects and the human, and does not model the explicit human-scene contact. Additionally, both [10, 87] do not model the coherence of human-scene interactions across frames from monocular video. In contrast to the prior work, our contribution lies in incorporating multiple human-scene interactions collectively, such that we can reconstruct a more accurate and consistent scene, with physically plausible human-scene interactions.

## 3. Method

MOVER is an optimization-based approach that reconstructs a physically plausible 3D scene that is consistent with predicted human-scene interactions over time (see Fig. 3). Specifically, our method takes an RGB video or multiple images $\{I_t\}_{t=1}^{T}$ as input and reconstructs the human bodies at each time step $t$ as well as the numerous static scene objects, all of which reside in a common 3D space and are supported by a ground plane. In our experiments, we consider indoor scenes containing large objects with which humans frequently interact, i.e., chairs, beds, sofas, and tables.

We initialize our approach using separate estimates for the 3D human poses [45, 66], the 3D scene [64], and the ground plane. Using the estimated body poses, we predict contact

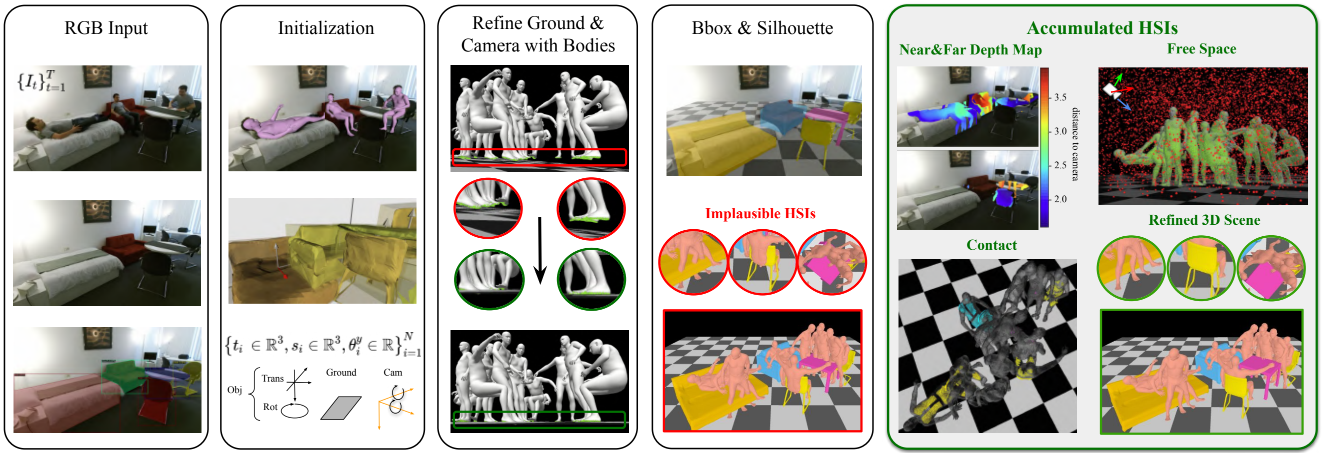


Figure 3. Overview of MOVER. Given a video/multiple images, the initialization involves using [64] to reconstruct a 3D scene from labeled or detected 2D instance segmentation masks [42], estimating the 3D human poses and shape [45, 66], and extracting the expected contact vertices on the estimated bodies using POSA [27]. The first step then refines the camera orientation and ground plane using the human bodies and their foot contact. Then we optimize the object layout based on 2D bounding boxes and silhouettes to remove interpenetration between people and objects, e.g., the human sits through the chair, stands in a table, or the legs penetrate a bed. Finally, incorporating multiple HSIs collectively from the whole video, we improve the 3D scene further such that the bodies perform more realistic HSIs.

vertices $\mathcal{C}$ for all bodies using POSA [27], which predicts likely contact vertices on the body conditioned on pose. We further divide these vertices into foot contacts $\mathcal{C}^{\text{feet}}$ and other body part contacts $\mathcal{C}^{\text{body}}$. The explicit foot contact points $\mathcal{C}^{\text{feet}}$ are used as constraints to refine the camera orientation and ground plane prediction. Based on this initialization, we optimize the alignment of the objects by minimizing an objective function based on multiple human-scene interactions (HSIs) across the entire input data.

### 3.1. 3D Scene Layout Optimization

Our method leverages multiple HSIs to refine the 3D scene. Recall that these HSIs provide the following constraints: (1) humans that move in a scene are occluded or occlude objects, thus, defining the depth ordering of the objects (depth order constraint), (2) humans move through free space and do not interpenetrate objects (collision constraint), (3) when humans and objects are in contact, the contact surfaces occupy the same place in space (contact constraint). Using these constraints, our objective is:

$$\begin{aligned}\mathcal{L}_{\text{scene-human}} &= \lambda_1 \mathcal{L}_{\text{bbox}} + \lambda_2 \mathcal{L}_{\text{occ-sil}} + \lambda_3 L_{\text{scale}} \\ &+ \lambda_4 \mathcal{L}_{\text{depth}} + \lambda_5 \mathcal{L}_{\text{collision}} + \lambda_6 \mathcal{L}_{\text{contact}}. \end{aligned} \quad (1)$$

We apply an occlusion-aware silhouette term $\mathcal{L}_{\text{occ-sil}}$ from [96], a 2D bounding box projection term $\mathcal{L}_{\text{bbox}}$ that constrains the top-left corner and the width of the bounding boxes of the objects, and $L_{\text{scale}}$, an $\ell_2$ regularizer to constrain object-scale variation, see more details in Sup. Mat.

**Depth Order Constraint $\mathcal{L}_{\text{depth}}$.** The occlusion between humans and objects can provide clues about the object's depth. We assume the human's depth is accurate. If a human occludes an object, then the far side of the person sets a limit on how close the object can be. Alternatively, if the object occludes the person, then the visible side of the person sets a maximum distance for the object. This is summarized in Fig. 4. In this way, human-object occlusion provides constraints on scene layout even when there is no human-object contact.

Directly applying the ordinal depth loss proposed by Jiang et al. [35] for each image is inefficient, as the required memory increases with the number of images. In contrast, we accumulate all single depth ordering maps into one far depth range map $\hat{D}_{\text{far}}$ and one near depth range map $\hat{D}_{\text{near}}$ as:

$$\begin{aligned}\hat{D}_{\text{far}}(p) &= \min\left(D^1_{\text{far}}(p), ..., D^T_{\text{far}}(p)\right), \\ \hat{D}_{\text{near}}(p) &= \max\left(D^1_{\text{near}}(p), ..., D^T_{\text{near}}(p)\right),\end{aligned}$$

where the pixel $p$ is in the overlapping region between the human bodies and the objects. Using these accumulated depth range maps, we constrain the depth $D_i(q)$ of a projected pixel $q$ from object $i$ to lie in the corresponding range:

$$\begin{aligned}\mathcal{L}_{\text{depth}} = \sum_i \sum_{q \in Sil_i \cap M_i} &[\text{ReLU}(D_i(q) - \hat{D}_{\text{far}}(q)) \\ &+ \text{ReLU}(\hat{D}_{\text{near}}(q) - D_i(q))],\end{aligned}$$

where $Sil_i$ is the rendered silhouette of the object $i$, $M_i$ is its 2D segmentation mask, and $D_i(q)$ is the depth of the object $i$ at the pixel $q$. See more details in Sup. Mat.

**Collision Constraint $\mathcal{L}_{\text{collision}}$.** To penalize all interpenetrating vertices of objects and bodies in the scene, we use

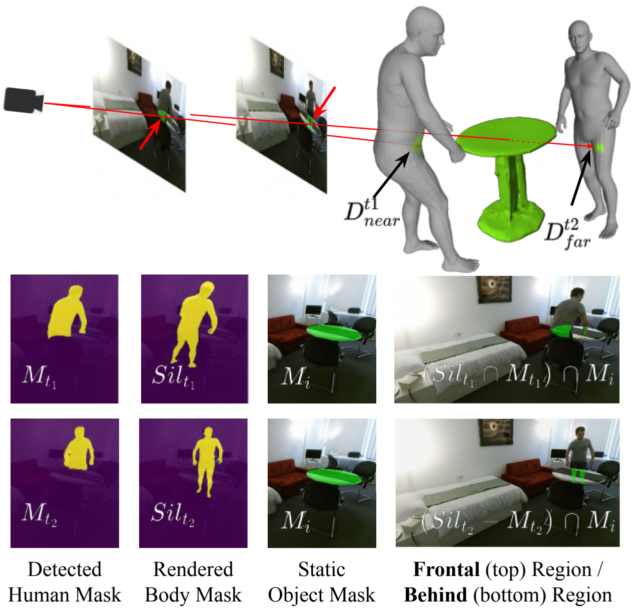


Figure 4. Computing depth range maps for the depth order constraint $\mathcal{L}_{\text{depth}}$. Given a detected human mask $M_t$ and a rendered body mask $Sil_t$, for each object $i$, we compute the overlap region between $M_i$ and $Sil_t \cap M_t$ as the frontal region and extract the depth of the backside surface of the body as the near depth range $D^t_{near}$ of the object $i$. Similarly, we compute $(Sil_t - M_t) \cap M_i$, which defines the far depth range $D^t_{far}$ of the object.

the signed distance field (SDF) of all reconstructed bodies. Specifically, we calculate a signed distance field volume $V_j$ for each body $j$ in a shared 3D world space, and accumulate them into a global SDF volume as $\hat{V} = \min(V_1, ..., V_j, ...)$. The SDF $\hat{V}$ is stored in a volumetric grid of size $256^3$, which spans a padded bounding box of all bodies. For a vertex $u_i$ of an object $O_i$, we compute the voxel coordinates $f(u_i) = (p(u_i), q(u_i), k(u_i))$ in the global SDF volume, and retrieve the corresponding SDF value $\hat{V}_{f(u_i)}$.

Based on the SDF values of all vertices of all $N$ objects, we resolve the scene-body interpenetration by penalizing vertices with a negative SDF value:

$$\mathcal{L}_{\text{collision}} = \sum_i \sum_u \|\hat{V}_{f(u_i)}\|_2^2, \quad \hat{V}_{f(u_i)} < 0.$$

**Contact Constraint $\mathcal{L}_{\text{contact}}$.** When humans and objects are in contact, the contact surfaces occupy the same place in space. We propose a contact constraint to minimize the distance between the contacted body parts and its assigned corresponding contacted object. PHOSA [96] proposes a loss in which they assign a whole body to only one object, whereas humans sometimes interact with multiple objects; e.g., a person sits on a chair and puts their hand on a table. In contrast, we directly assign the contacted body vertices $\mathcal{C}_i^{body}$ of each body to different objects, based on the overlap between the 2D projection of the vertices and the detected object masks, and based on the 3D distances between them. We consider the vertices of sofa and chair backs and seat bottoms as contactable regions, see more details in Sup. Mat.

We minimize the distance between the contacted bodies and the contacted object parts:

$$\mathcal{L}_{\text{contact}} = \sum_i \sum_{v \in \mathcal{C}^{\text{body}}} \mathbb{I}(v, O_i)[\text{CD}(v^y, \mathcal{C}(O_i)^y) + \text{CD}(v^{\perp y}, \mathcal{C}(O_i)^{\perp y})],$$

where $\mathcal{C}(O_i)^{\perp y}$ and $\mathcal{C}(O_i)^y$ denote the back and the bottom seat contact part of an object $i$, respectively, $y$ denotes the y-axis direction and $\perp y$ the vertical direction to it. $\mathbb{I}(v, O_i)$ is an indicator function (1 only if the contact vertex $v$ is assigned to the contacted object $O_i$, 0 else). CD denotes the one-directional Chamfer Distance (CD), i.e., from bodies to objects, because for large furniture like a bed or a sofa, a human only contacts a small region of the object. In contrast, PHOSA [96] uses a bi-directional CD, which tends to shrink the object to match the contacted body parts.

### 3.2. Optimization

We optimize Eq. (1) for a specific scene w.r.t. the parameters $\mathbf{s}_i$ (scale), $\theta_i$ (rotation), $\mathbf{t}_i$ (translation) of the objects $\{i = 1...N\}$, with the Adam optimizer [41]. In the following, we detail the initialization of the 3D scene and the HPS.

**Initial 3D Scene.** We extract a representative 2D image $\mathbf{I}$ from the input data without any human-object occlusion. For this image, depending on the experiment, we either use the ground truth 2D bounding boxes $B_i$ and instance masks $M_i$ for all $N$ objects in the scene or compute them using PointRend [42]. We use [64] to get an initial 3D scene $\mathbf{S}_0$, consisting of a ground plane $y = y_{gp}$ and multiple object meshes $\{O_i\}_{i=1}^N$, and a perspective camera with *roll* and *pitch*. Each object $i$ has a translation $\mathbf{t}_i \in \mathbb{R}^3$, scale $\mathbf{s}_i \in \mathbb{R}^3$, and a rotation around the y-axis $\theta_i^y \in [0, 2\pi)$. Since the predicted meshes of [64] are incomplete and have holes, we use Occupancy Networks [61] and Marching Cubes [57] to transform each object mesh into a water-tight mesh. Based on this preparation, we first optimize the objective function without considering the HSIs:

$$\mathcal{L}_{\text{scene}} = \mathcal{L}_{\text{occ-sil}} + \lambda_1 \mathcal{L}_{\text{bbox}} + \lambda_2 \mathcal{L}_{\text{scale}}.$$

**Initialization of the ground and camera.** As shown in the third column of Fig. 3, the estimated ground plane and camera orientation from [64] are inconsistent with the reconstructed bodies (e.g., people float in the air). Previous methods either fix the camera orientation and only optimize the ground plane and humans [10], or estimate them independently per image [87], which generates inconsistent camera orientations and ground planes throughout a video. However, the camera orientation and ground plane are essential for producing plausible HSIs. Thus, we jointly estimate the ground, camera and multiple humans together, by applying:

$$\mathcal{L}_{\text{feet}}(R, p) = \rho(R^\top \sum_t \mathcal{C}_t^{\text{feet}} - [0, y_{gp}, 0]^\top; \sigma_1),$$

where $R$ is the camera rotation matrix calculated from *pitch*, and *roll*, and $\rho$ denotes a robust Geman-McClure error function [15] for down-weighting outliers and $\sigma_1 = 0.1$.

**Initial Estimate of 3D Bodies.** To obtain an initial body shape and pose estimate for the input images $\{I_t\}_{t=1}^T$, we use OpenPose [7] and SMPLify-X [66]. Specifically, we use a perspective camera and estimate the pose parameters $\theta_t$ of SMPL-X for each frame with shared body shape parameters $\beta$. SMPLify-X requires a good initialization and, for this, we use PARE [45] because it is robust to occlusion and our scenes involve significant occlusion. PARE outputs SMPL, which we convert to SMPL-X [1], and use the resulting 3D joints to initialize SMPLify-X, see more details in Sup. Mat.

We then optimize all SMPL-X parameters to minimize an objective function $E_{\text{Body}}$ of multiple terms, as described in SMPLify-X [66] (see $E_{\text{SMPLify-X}}$) :

$$E_{\text{Body}} = \sum_{t=1}^{T} (E_{\text{SMPLify-X}}(t)) + \lambda_{\text{smooth}} \mathcal{L}_{\text{smooth}}.$$

To reduce jitter, we add a constant-velocity motion smoothing term on 3D joints $J$ and their 2D projections $J^{\text{Proj}}$:

$$\mathcal{L}_{\text{smooth}} = \sum_{t=1}^{T-1} \rho\left(\|J_{t-1} + J_{t+1} - 2 \times J_t\|; \sigma_2\right) + \rho\left(\|J_{t-1}^{\text{Proj}} + J_{t+1}^{\text{Proj}} - 2 \times J_t^{\text{Proj}}\|; \sigma_3\right),$$

where $\sigma_2 = 0.1$ and $\sigma_3 = 100$. To avoid noisy and unreliable body poses, and therefore, incorrect human-scene interactions during optimization, we also filter out outliers based on a constant-velocity assumption. To that end, we calculate the acceleration of the pelvis $\nu_t$ and the joints $\alpha_t$ of a person in frame $t$. We filter out frames in which either pelvis translation or joint velocities are above a threshold; that is, $\{j : \nu_j < \tau_{\text{pelvis}} \cap \alpha_j < \tau_{\text{local}}, j \in \{1...T\}\}$, where $\tau_{pel}$, $\tau_{local}$ are the thresholds for the pelvis acceleration and the local pose acceleration, respectively.

# 4. Experiments

To evaluate the influence of accumulated HSIs on the optimized 3D scene layout, we use two different datasets, PiGraphs [74] and PROX [26] (see Sup. Mat.). In comparison to [64] and [87], we achieve state-of-the-art 3D scene layout reconstruction, both quantitatively (see Sec. 4.1) and qualitatively (see Sec. 4.3). On the PROX *quantitative* dataset, we find that our 3D scene reconstructions lead to more accurate human shape and pose estimations than our baselines. In Sec. 4.2, we analyze the different energy terms and how they contribute to our final results.

## 4.1. Quantitative Analysis

We perform several experiments to investigate the effectiveness of our proposed method in three parts: 3D scene reconstruction, human-scene interaction (HSI) reconstruction, and human pose and shape (HPS) estimation.

**3D Scene Reconstruction.** Following [10, 32, 64, 87], we compute the 3D IoU and 2D IoU of object bounding boxes to evaluate the 3D scene reconstruction and the consistency between the 3D world and 2D image on PROX and PiGraphs. However, the 3D IoU is coarse and does not capture the error in an object's orientation, which is quite important for physically plausible HSI, e.g., a human can not sit on an armed chair with the wrong orientation. Therefore, we introduce the *point2surface distance* ($p2s$) to measure the distance from a cropped object mesh to the estimated 3D object mesh. It enables 3D scene reconstruction evaluation with more geometric details including orientation and shape. Given 2D labeled or detected [42] bounding boxes and masks, our method improves the input [64] significantly, and outperforms [87] on all scene-reconstruction metrics and different datasets, as shown in Tab. 2 and Tab. 3.

Furthermore, we evaluate the error of the camera orientation and ground plane penetration [68] using the estimated foot contact vertices (see Tab. 4). We find that jointly optimizing the camera orientation and the ground plane using foot contact significantly improves accuracy compared to the initial estimate from [64].

**Human-scene Interaction Reconstruction.** To evaluate the physical plausibility of the estimated scene, we compute the metrics used in prior work [27, 98, 99]. Specifically, for each reconstructed body and 3D scene, we calculate (1) the *non-collision score* to measure the ratio of body mesh vertices that do not penetrate the estimated 3D scene, divided by the number of all body mesh vertices, and (2) the *contact score* to denote whether the body is in contact with the 3D scene or not. The *contact score* is 1, if at least one vertex of a body interpenetrates the 3D scene. We report the mean *non-collision score* and mean *contact scores* among all videos and all bodies. In Tab. 2, MOVER achieves the best balance between non-collision and contact.

The estimated scenes with detected 2D boxes and masks [42] provide lower HSI scores than with 2D GT. This is mainly because of the mis-detected objects from [42]. Since the reconstructed scenes of [87] do not support human-scene contact well, e.g., a sitting body often floats, due to the lack of explicit human-scene contact modeling, it has a better non-collision score but a lower contact score.

| Methods | Setting | | | | | Scene Recon. | | | HSI | |
|---|---|---|---|---|---|---|---|---|---|---|
| | BBOX&Mask | Cam. | Contact | Depth | Colli. | $\text{IoU}_{3D}\uparrow$ | P2S$\downarrow$ | $\text{IoU}_{2D}\uparrow$ | Non-Col $\uparrow$ | Cont. $\uparrow$ |
| HolisticMesh [87] | PointRend | | | | | 0.211 | 0.410 | 0.648 | 0.990 | 0.369 |
| Total3D [64] | PointRend | | | | | 0.246 | 0.319 | 0.522 | 0.974 | 0.510 |
| **Ours** | PointRend | ✓ | ✓ | ✓ | ✓ | 0.309 | 0.221 | 0.777 | 0.977 | 0.612 |
| HolisticMesh [87] | 2D GT | | | | | 0.267 | 0.237 | 0.745 | 0.988 | 0.491 |
| Total3D [64] | 2D GT | | | | | 0.196 | 0.369 | 0.227 | 0.963 | 0.440 |
| **Ours** | 2D GT | ✓ | ✓ | ✓ | ✓ | 0.383 | 0.199 | 0.898 | 0.986 | 0.673 |
| Ablation Study | 2D GT | ✓ | | | | 0.374 | 0.206 | 0.859 | 0.979 | 0.738 |
| | | ✓ | ✓ | ✓ | | 0.389 | 0.199 | 0.904 | 0.983 | 0.697 |
| | | ✓ | ✓ | | | 0.381 | 0.205 | 0.904 | 0.980 | 0.773 |
| | | ✓ | | ✓ | | 0.393 | 0.194 | 0.907 | 0.983 | 0.638 |
| | | ✓ | | | ✓ | 0.383 | 0.199 | 0.903 | 0.984 | 0.674 |

Table 2. Quantitative results for 3D scene understanding (3D object detection) and human-scene interaction on the PROX *qualitative* dataset. P2S, Non-Col and Cont denote *point2surface distance*, Non-Collision and Contactness respectively. In each column, red is the best result among methods that take 2D labeled masks as input; blue is the second best. The check marks indicate which constraints are used.

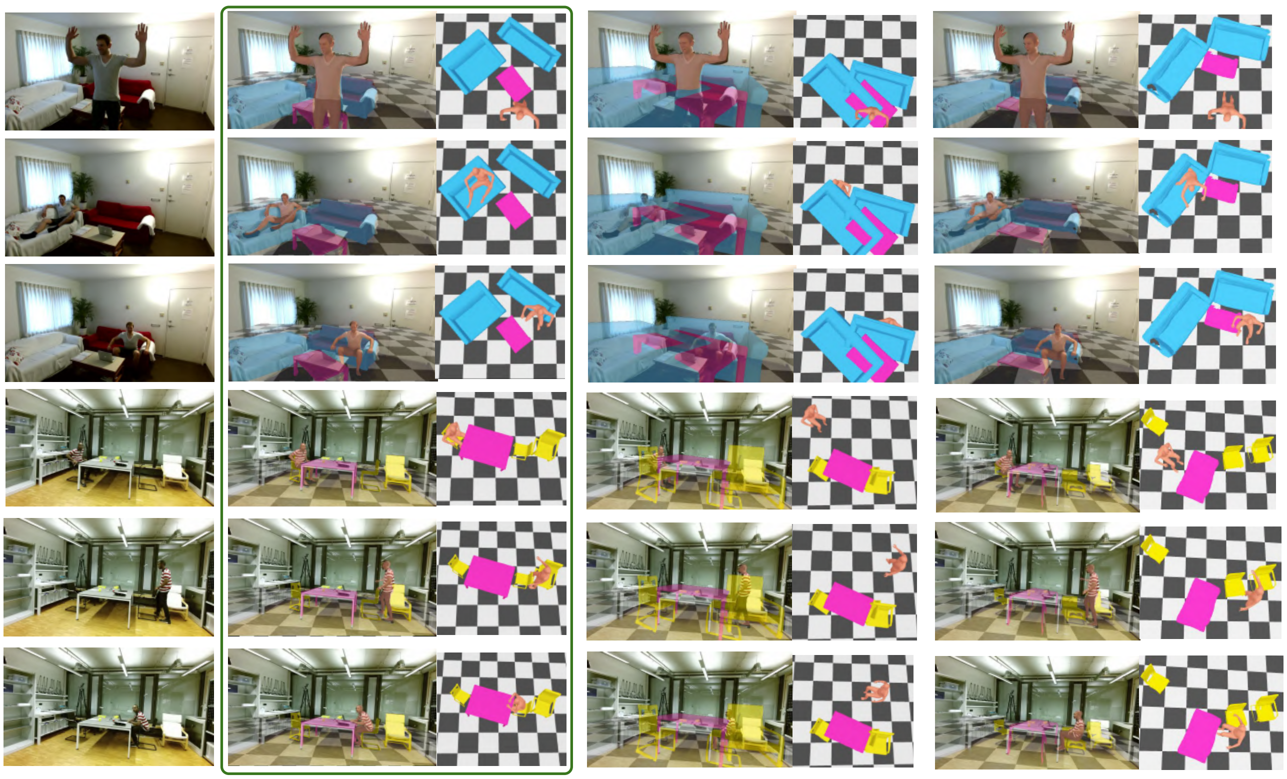


Figure 5. Qualitative results on PiGraphs [74] (top) and PROX [26] (bottom). Our method recovers better 3D scenes and HPS, which supports more plausible HSIs, compared with two baselines: Total3D [64] and HolisticMesh [87].

**Human Pose and Shape (HPS) Estimation.** Can we use the estimated 3D scene to, in turn, improve 3D HPS? Here we follow PROX but replace the scanned 3D scene of PROX with our estimated 3D scene. In Tab. 5, we evaluate the HPS estimation on PROX *quantitative* using the metrics from [26]. Specifically, we report (1) the mean per-joint error (PJE) and (2) the mean vertex-to-vertex distance (V2V). Unlike the common measures in the field, neither of these metrics align the body with ground truth, either at the pelvis or using full Procrustes alignment. For completeness, we also compute these metrics with Procrustes alignment, denoted as p.PJE and p.V2V, respectively. Note that the metrics w./o. Pro-

| Methods | $\text{IoU}_{2D}$ ↑ | $\text{IoU}_{3D}$ ↑ |
|---|---|---|
| Cooperative [31] | 68.6 | 21.4 |
| Holistic++ [10] | 75.1 | 24.9 |
| HolisticMesh [87] | 75.6 | 26.3 |
| **Ours** | **79.2** | **27.8** |

Table 3. Quantitative results for 3D scene understanding (3D object detection) on *PiGraphs* dataset [74].

| | Cam. Orien. | | | Ground Pen | |
|---|---|---|---|---|---|
| Methods | pitch ↓ | roll ↓ | mean ↓ | Freq. ↓ | Dist. ↓ |
| Total3D [64] | 0.059 | **0.031** | 0.045 | 0.316 | 0.167 |
| **Ours** | **0.042** | 0.034 | **0.038** | **0.100** | **0.112** |

Table 4. Errors in the camera orientation and the ground penetration using foot contact on the PROX *qualitative* dataset.

crustes alignment (PJE and V2V) are more meaningful here, since we want to evaluate how well the method solves for the translation, rotation, and scaling of the human body. As shown in Tab. 5, with estimated camera orientation and ground plane constraints (+CamGP), the PJE and V2V are both improved by a significant margin $+43.21$ and $+42.41$ respectively, w.r.t. our baseline. We also see that our refined scene can further refine our estimated bodies by applying the SDF loss (+SDF) and the contact loss (+Contact) from [26]. Our final body estimation outperforms HolisticMesh [87] and is similar to PROX, *without having access to a scanned 3D scene.*

### 4.2. Ablation Study

To analyze the contribution of the accumulated HSIs and the different constraints, we conducted multiple ablation studies; see Tab. 2. All three proposed HSI constraints (depth order, collision, and contact) help to improve 3D scene reconstruction in different ways. The *contact* constraint produces the highest human-scene contact scores, but decreases the non-collision score. The *collision* and *depth order* both contribute to the non-collision score. However, using only the *depth order* constraint achieves a slightly better 3D scene than our full model, but leads to worse human-scene contact scores. By applying all constraints, our method can generate a 3D scene that supports more physically plausible HSIs.

### 4.3. Qualitative Analysis

In Fig. 5, we show reconstructed 3D scenes and humans along with frames from the RGB videos, to demonstrate the effectiveness and generality of our approach on different datasets (PROX [26] and PiGraphs [74]). MOVER recovers better 3D scenes and HPS compared to Total3D [64] and HolisticMesh [87]. See Sup. Mat. for more examples.

| Methods | PJE↓ | V2V ↓ | p.PJE ↓ | p.V2V↓ |
|---|---|---|---|---|
| With **G.T Captured 3D Scene Scans** | | | | |
| RGB [26] | 220.27 | 218.06 | 73.24 | 60.80 |
| PROX [26] | 167.08 | 166.51 | 71.97 | 61.14 |
| With **Image2Mesh Models** | | | | |
| HolisticMesh [87] | 190.78 | 192.21 | **72.72** | **61.01** |
| baseline* | 219.62 | 222.50 | 75.92 | 68.34 |
| +CamGP | 176.41 | 180.09 | 73.41 | 67.33 |
| +CamGP+SDF | 175.98 | 179.98 | 73.96 | 68.29 |
| **Ours** | **174.37** | **178.31** | 73.60 | 67.89 |

Table 5. Quantitative results for human pose estimation on PROX *quantitative* dataset (baseline* denotes batch-wise SMPLify-X, **Ours**: +CamGP+SDF+Contact.)

## 5. Discussion

Based on single-view inputs, our proposed method optimizes the 3D pose of objects in a scene. While we assume a static camera, future work should explore moving cameras and structure-from-motion techniques to better estimate the 3D scene. We also assume that the scene is static. However, humans move objects when interacting with the world, resulting in a dynamic scene layout. We believe that our proposed constraints based on HSIs will be beneficial for future work on reconstructing dynamic scenes. Besides optimizing the 3D scene layout, we do not change the initial shape estimate of an object. A more flexible and adjustable geometric object representation, e.g., an implicit representation, would be beneficial. One could then optimize over the space of object shapes in addition to object poses. While here we focus on large objects like furniture, hand-held objects are also important and are likely subject to different constraints. During HSI, bodies are often occluded, causing errors in estimated 3D human pose. These estimates could be improved by incorporating strong human motion priors [68, 97].

## 6. Conclusion

We have introduced MOVER, which reconstructs a 3D scene by exploiting 3D humans interacting with it. We have demonstrated that accumulated HSIs, computed from a monocular video, can be leveraged to improve the 3D reconstruction of a scene. The reconstructed scene, in turn, can be used to improve 3D human pose estimation. In contrast to the state of the art, MOVER can reconstruct a consistent, physically plausible 3D scene layout.

**Acknowledgments.** We thank Yixin Chen, Yuliang Xiu for the insightful discussions, Yao Feng, Partha Ghosh and Maria Paola Forte for proof-reading, and Benjamin Pellkofer for IT support. This work was supported by the German Federal Ministry of Education and Research (BMBF): Tübingen AI Center, FKZ: 01IS18039B.

**Disclosure.** https://files.is.tue.mpg.de/black/CoI_CVPR_2022.txt

## References


[1] https://github.com/vchoutas/smplx/tree/master/transfer_model. 6

[2] Mykhaylo Andriluka, Umar Iqbal, Eldar Insafutdinov, Leonid Pishchulin, Anton Milan, Juergen Gall, and Bernt Schiele. PoseTrack: A benchmark for human pose estimation and tracking. In *Computer Vision and Pattern Recognition (CVPR)*, pages 5167–5176, 2018. 2

[3] Dragomir Anguelov, Praveen Srinivasan, Daphne Koller, Sebastian Thrun, Jim Rodgers, and James Davis. SCAPE: Shape Completion and Animation of PEople. *Transactions on Graphics (TOG)*, 24(3):408–416, 2005. 2

[4] Aayush Bansal, Bryan Russell, and Abhinav Gupta. Marr revisited: 2D-3D alignment via surface normal prediction. In *Computer Vision and Pattern Recognition (CVPR)*, pages 5965–5974, 2016. 3

[5] Federica Bogo, Angjoo Kanazawa, Christoph Lassner, Peter Gehler, Javier Romero, and Michael J. Black. Keep it SMPL: Automatic estimation of 3D human pose and shape from a single image. In *European Conference on Computer Vision (ECCV)*, pages 561–578, 2016. 3

[6] Aljaž Božič, Pablo Palafox, Justus Thies, Angela Dai, and Matthias Nießner. TransformerFusion: Monocular RGB scene reconstruction using transformers. In *Conference on Neural Information Processing Systems (NeurIPS)*, 2021. 1

[7] Zhe Cao, Gines Hidalgo Martinez, Tomas Simon, Shih-En Wei, and Yaser Sheikh. OpenPose: Realtime multi-person 2D pose estimation using part affinity fields. *Transactions on Pattern Analysis and Machine Intelligence (TPAMI)*, 43(1):172–186, 2021. 2, 6

[8] Zhe Cao, Ilija Radosavovic, Angjoo Kanazawa, and Jitendra Malik. Reconstructing hand-object interactions in the wild. In *International Conference on Computer Vision (ICCV)*, pages 12417–12426, 2021. 3

[9] Yu-Wei Chao, Wei Yang, Yu Xiang, Pavlo Molchanov, Ankur Handa, Jonathan Tremblay, Yashraj S Narang, Karl Van Wyk, Umar Iqbal, Stan Birchfield, et al. DexYCB: A benchmark for capturing hand grasping of objects. In *Computer Vision and Pattern Recognition (CVPR)*, pages 9044–9053, 2021. 3

[10] Yixin Chen, Siyuan Huang, Tao Yuan, Yixin Zhu, Siyuan Qi, and Song-Chun Zhu. Holistic++ scene understanding: Single-view 3D holistic scene parsing and human pose estimation with human-object interaction and physical commonsense. In *International Conference on Computer Vision (ICCV)*, pages 8647–8656, 2019. 1, 2, 3, 5, 6, 8

[11] Wongun Choi, Yu-Wei Chao, Caroline Pantofaru, and Silvio Savarese. Understanding indoor scenes using 3D geometric phrases. In *Computer Vision and Pattern Recognition (CVPR)*, pages 33–40, 2013. 3

[12] Vasileios Choutas, Lea Müller, Chun-Hao P. Huang, Siyu Tang, Dimitrios Tzionas, and Michael J. Black. Accurate 3D body shape regression via linguistic attributes and anthropometric measurements. In *Computer Vision and Pattern Recognition (CVPR)*, 2022. 1

[13] Vasileios Choutas, Georgios Pavlakos, Timo Bolkart, Dimitrios Tzionas, and Michael J. Black. Monocular expressive body regression through body-driven attention. In *European Conference on Computer Vision (ECCV)*, pages 20–40, 2020. 3

[14] Christopher B Choy, Danfei Xu, JunYoung Gwak, Kevin Chen, and Silvio Savarese. 3D-R2N2: A unified approach for single and multi-view 3D object reconstruction. In *European Conference on Computer Vision (ECCV)*, pages 628–644, 2016. 3

[15] M Comer, C Bouman, and J Simmons. Statistical methods for image segmentation and tomography reconstruction. *Microscopy and Microanalysis*, 16(S2):1852–1853, 2010. 6

[16] Rishabh Dabral, Soshi Shimada, Arjun Jain, Christian Theobalt, and Vladislav Golyanik. Gravity-aware monocular 3D human-object reconstruction. In *International Conference on Computer Vision (ICCV)*, pages 12365–12374, 2021. 3

[17] Manuel Dahnert, Ji Hou, , Matthias Nießner, and Angela Dai. Panoptic 3D scene reconstruction from a single RGB image. In *Conference on Neural Information Processing Systems (NeurIPS)*, 2021. 1, 3

[18] Saumitro Dasgupta, Kuan Fang, Kevin Chen, and Silvio Savarese. DeLay: Robust spatial layout estimation for cluttered indoor scenes. In *Computer Vision and Pattern Recognition (CVPR)*, pages 616–624, 2016. 3

[19] Maximilian Denninger and Rudolph Triebel. 3D scene reconstruction from a single viewport. In *European Conference on Computer Vision (ECCV)*, pages 51–67, 2020. 3

[20] Huan Fu, Mingming Gong, Chaohui Wang, Kayhan Batmanghelich, and Dacheng Tao. Deep ordinal regression network for monocular depth estimation. In *Computer Vision and Pattern Recognition (CVPR)*, pages 2002–2011, 2018. 3

[21] Valentin Gabeur, Jean-Sebastien Franco, Xavier Martin, Cordelia Schmid, and Gregory Rogez. Moulding Humans: Non-parametric 3D human shape estimation from single images. In *International Conference on Computer Vision (ICCV)*, pages 2232–2241, 2019. 2

[22] Georgia Gkioxari, Jitendra Malik, and Justin Johnson. Mesh R-CNN. In *International Conference on Computer Vision (ICCV)*, pages 9785–9795, 2019. 3

[23] Clément Godard, Oisin Mac Aodha, and Gabriel J Brostow. Unsupervised monocular depth estimation with left-right consistency. In *Computer Vision and Pattern Recognition (CVPR)*, pages 270–279, 2017. 3

[24] Thibault Groueix, Matthew Fisher, Vladimir G. Kim, Bryan Russell, and Mathieu Aubry. AtlasNet: A papier-mâché approach to learning 3D surface generation. In *CVPR*, pages 216–224, 2018. 3

[25] Nils Hasler, Carsten Stoll, Martin Sunkel, Bodo Rosenhahn, and Hans-Peter Seidel. A statistical model of human pose and body shape. *Computer Graphics Forum*, 28(2):337–346, 2009. 2

[26] Mohamed Hassan, Vasileios Choutas, Dimitrios Tzionas, and Michael J. Black. Resolving 3D human pose ambiguities with 3D scene constraints. In *International Conference on Computer Vision (ICCV)*, pages 2282–2292, 2019. 1, 2, 3, 6, 7, 8

[27] Mohamed Hassan, Partha Ghosh, Joachim Tesch, Dimitrios Tzionas, and Michael J. Black. Populating 3D scenes by learning human-scene interaction. In *Computer Vision and*

*Pattern Recognition (CVPR)*, pages 14708–14718, 2021. 2, 3, 4, 6

[28] Kaiming He, Georgia Gkioxari, Piotr Dollár, and Ross Girshick. Mask R-CNN. In *International Conference on Computer Vision (ICCV)*, pages 2961–2969, 2017. 3

[29] Varsha Hedau, Derek Hoiem, and David Forsyth. Recovering the spatial layout of cluttered rooms. In *International Conference on Computer Vision (ICCV)*, pages 1849–1856, 2009. 3

[30] Chun-Hao P. Huang, Hongwei Yi, Markus Höschle, Matvey Safroshkin, Tsvetelina Alexiadis, Senya Polikovsky, Daniel Scharstein, and Michael J. Black. Capturing and inferring dense full-body human-scene contact. In *Computer Vision and Pattern Recognition (CVPR)*, 2022. 3

[31] Siyuan Huang, Siyuan Qi, Yinxue Xiao, Yixin Zhu, Ying Nian Wu, and Song-Chun Zhu. Cooperative holistic scene understanding: Unifying 3D object, layout, and camera pose estimation. In *Conference on Neural Information Processing Systems (NeurIPS)*, pages 207–218, 2018. 1, 3, 8

[32] Siyuan Huang, Siyuan Qi, Yixin Zhu, Yinxue Xiao, Yuanlu Xu, and Song-Chun Zhu. Holistic 3D scene parsing and reconstruction from a single RGB image. In *European Conference on Computer Vision (ECCV)*, pages 194–211, 2018. 3, 6

[33] Hamid Izadinia, Qi Shan, and Steven M Seitz. IM2CAD. In *Computer Vision and Pattern Recognition (CVPR)*, pages 5134–5143, 2017. 3

[34] Hanwen Jiang, Shaowei Liu, Jiashun Wang, and Xiaolong Wang. Hand-object contact consistency reasoning for human grasps generation. In *International Conference on Computer Vision (ICCV)*, pages 11107–11116, 2021. 3

[35] Wen Jiang, Nikos Kolotouros, Georgios Pavlakos, Xiaowei Zhou, and Kostas Daniilidis. Coherent reconstruction of multiple humans from a single image. In *Computer Vision and Pattern Recognition (CVPR)*, pages 5579–5588, 2020. 4

[36] Sheng Jin, Lumin Xu, Jin Xu, Can Wang, Wentao Liu, Chen Qian, Wanli Ouyang, and Ping Luo. Whole-body human pose estimation in the wild. In *European Conference on Computer Vision (ECCV)*, pages 196–214, 2020. 2

[37] Hanbyul Joo, Natalia Neverova, and Andrea Vedaldi. Exemplar fine-tuning for 3D human pose fitting towards in-the-wild 3D human pose estimation. In *International Conference on 3D Vision (3DV)*, pages 42–52, 2020. 1, 3

[38] Hanbyul Joo, Tomas Simon, and Yaser Sheikh. Total capture: A 3D deformation model for tracking faces, hands, and bodies. In *Computer Vision and Pattern Recognition (CVPR)*, pages 8320–8329, 2018. 2, 3

[39] Angjoo Kanazawa, Michael J. Black, David W. Jacobs, and Jitendra Malik. End-to-end recovery of human shape and pose. In *Computer Vision and Pattern Recognition (CVPR)*, pages 7122–7131, 2018. 1, 3

[40] Rawal Khirodkar, Shashank Tripathi, and Kris Kitani. Occluded human mesh recovery. In *Computer Vision and Pattern Recognition (CVPR)*, 2022. 3

[41] Diederik P. Kingma and Jimmy Ba. Adam: A method for stochastic optimization. *arXiv preprint arXiv:1412.6980*, pages 273–297, 2014. 5

[42] Alexander Kirillov, Yuxin Wu, Kaiming He, and Ross Girshick. PointRend: Image segmentation as rendering. In *Computer Vision and Pattern Recognition (CVPR)*, pages 9799–9808, 2020. 2, 4, 5, 6

[43] Hedvig Kjellström, Danica Kragić, and Michael J Black. Tracking people interacting with objects. In *Computer Vision and Pattern Recognition (CVPR)*, pages 747–754, 2010. 3

[44] Muhammed Kocabas, Nikos Athanasiou, and Michael J. Black. VIBE: Video inference for human body pose and shape estimation. In *Computer Vision and Pattern Recognition (CVPR)*, pages 5253–5263, 2020. 1, 3

[45] Muhammed Kocabas, Chun-Hao P. Huang, Otmar Hilliges, and Michael J. Black. PARE: Part attention regressor for 3D human body estimation. In *Computer Vision and Pattern Recognition (CVPR)*, pages 11127–11137, 2021. 1, 2, 3, 4, 6

[46] Nikos Kolotouros, Georgios Pavlakos, Michael J. Black, and Kostas Daniilidis. Learning to reconstruct 3D human pose and shape via model-fitting in the loop. In *International Conference on Computer Vision (ICCV)*, pages 2252–2261, 2019. 1, 3

[47] Nikos Kolotouros, Georgios Pavlakos, and Kostas Daniilidis. Convolutional mesh regression for single-image human shape reconstruction. In *Computer Vision and Pattern Recognition (CVPR)*, pages 4496–4505, 2019. 2

[48] Weicheng Kuo, Anelia Angelova, Tsung-Yi Lin, and Angela Dai. Mask2CAD: 3D shape prediction by learning to segment and retrieve. In *European Conference on Computer Vision (ECCV)*, pages 260–277, 2020. 3

[49] Taein Kwon, Bugra Tekin, Jan Stühmer, Federica Bogo, and Marc Pollefeys. H2O: Two hands manipulating objects for first person interaction recognition. In *International Conference on Computer Vision (ICCV)*, pages 10138–10148, 2021. 3

[50] Iro Laina, Christian Rupprecht, Vasileios Belagiannis, Federico Tombari, and Nassir Navab. Deeper depth prediction with fully convolutional residual networks. In *International Conference on 3D Vision (3DV)*, pages 239–248, 2016. 3

[51] David C Lee, Martial Hebert, and Takeo Kanade. Geometric reasoning for single image structure recovery. In *Computer Vision and Pattern Recognition (CVPR)*, pages 2136–2143, 2009. 3

[52] Xueting Li, Sifei Liu, Kihwan Kim, Xiaolong Wang, Ming-Hsuan Yang, and Jan Kautz. Putting humans in a scene: Learning affordance in 3D indoor environments. In *Computer Vision and Pattern Recognition (CVPR)*, pages 12368–12376, 2019. 3

[53] Zongmian Li, Jiri Sedlar, Justin Carpentier, Ivan Laptev, Nicolas Mansard, and Josef Sivic. Estimating 3D motion and forces of person-object interactions from monocular video. In *Computer Vision and Pattern Recognition (CVPR)*, pages 8640–8649, 2019. 3

[54] Shaowei Liu, Hanwen Jiang, Jiarui Xu, Sifei Liu, and Xiaolong Wang. Semi-supervised 3D hand-object poses estimation with interactions in time. In *Computer Vision and Pattern Recognition (CVPR)*, pages 14687–14697, 2021. 3

[55] Shaohui Liu, Yinda Zhang, Songyou Peng, Boxin Shi, Marc Pollefeys, and Zhaopeng Cui. Dist: Rendering deep implicit signed distance function with differentiable sphere tracing.

In *Computer Vision and Pattern Recognition (CVPR)*, pages 2019–2028, 2020. 3

[56] Matthew Loper, Naureen Mahmood, Javier Romero, Gerard Pons-Moll, and Michael J. Black. SMPL: A skinned multi-person linear model. *Transactions on Graphics (TOG)*, 34(6):248:1–248:16, 2015. 2

[57] William E. Lorensen and Harvey E. Cline. Marching cubes: A high resolution 3D surface construction algorithm. *International Conference on Computer Graphics and Interactive Techniques (SIGGRAPH)*, 21(4):163–169, 1987. 5

[58] Zhengyi Luo, Ryo Hachiuma, Ye Yuan, and Kris Kitani. Dynamics-regulated kinematic policy for egocentric pose estimation. In *Conference on Neural Information Processing Systems (NeurIPS)*, 2021. 1

[59] Arun Mallya and Svetlana Lazebnik. Learning informative edge maps for indoor scene layout prediction. In *International Conference on Computer Vision (ICCV)*, pages 936–944, 2015. 3

[60] Julieta Martinez, Rayat Hossain, Javier Romero, and James J. Little. A simple yet effective baseline for 3D human pose estimation. In *International Conference on Computer Vision (ICCV)*, pages 2659–2668, 2017. 2

[61] Lars Mescheder, Michael Oechsle, Michael Niemeyer, Sebastian Nowozin, and Andreas Geiger. Occupancy networks: Learning 3D reconstruction in function space. In *Computer Vision and Pattern Recognition (CVPR)*, pages 4460–4470, 2019. 3, 5

[62] Thomas B. Moeslund, Adrian Hilton, and Volker Krüger. A survey of advances in vision-based human motion capture and analysis. *Computer Vision and Image Understanding (CVIU)*, 104(2):90–126, 2006. 2

[63] Aron Monszpart, Paul Guerrero, Duygu Ceylan, Ersin Yumer, and Niloy J Mitra. iMapper: interaction-guided scene mapping from monocular videos. *Transactions on Graphics (TOG)*, 38(4):92:1–92:15, 2019. 3

[64] Yinyu Nie, Xiaoguang Han, Shihui Guo, Yujian Zheng, Jian Chang, and Jian Jun Zhang. Total3DUnderstanding: Joint layout, object pose and mesh reconstruction for indoor scenes from a single image. In *Computer Vision and Pattern Recognition (CVPR)*, pages 55–64, 2020. 1, 2, 3, 4, 5, 6, 7, 8

[65] Jeong Joon Park, Peter Florence, Julian Straub, Richard Newcombe, and Steven Lovegrove. DeepSDF: Learning continuous signed distance functions for shape representation. In *Computer Vision and Pattern Recognition (CVPR)*, pages 165–174, 2019. 3

[66] Georgios Pavlakos, Vasileios Choutas, Nima Ghorbani, Timo Bolkart, Ahmed AA Osman, Dimitrios Tzionas, and Michael J. Black. Expressive body capture: 3D hands, face, and body from a single image. In *Computer Vision and Pattern Recognition (CVPR)*, pages 10975–10985, 2019. 1, 2, 3, 4, 6

[67] Georgios Pavlakos, Nikos Kolotouros, and Kostas Daniilidis. TexturePose: Supervising human mesh estimation with texture consistency. In *International Conference on Computer Vision (ICCV)*, pages 803–812, 2019. 1

[68] Davis Rempe, Tolga Birdal, Aaron Hertzmann, Jimei Yang, Srinath Sridhar, and Leonidas J. Guibas. HuMoR: 3D human motion model for robust pose estimation. In *International Conference on Computer Vision (ICCV)*, pages 11488–11499, 2021. 6, 8

[69] Grégory Rogez and Cordelia Schmid. MoCap-guided data augmentation for 3D pose estimation in the wild. In *Conference on Neural Information Processing Systems (NeurIPS)*, pages 3108–3116, 2016. 2

[70] Javier Romero, Dimitrios Tzionas, and Michael J. Black. Embodied hands: Modeling and capturing hands and bodies together. *Transactions on Graphics (TOG)*, 36(6):245:1–245:17, 2017. 2

[71] Shunsuke Saito, Zeng Huang, Ryota Natsume, Shigeo Morishima, Angjoo Kanazawa, and Hao Li. PIFu: Pixel-aligned implicit function for high-resolution clothed human digitization. In *International Conference on Computer Vision (ICCV)*, pages 2304–2314, 2019. 2, 3

[72] Shunsuke Saito, Tomas Simon, Jason Saragih, and Hanbyul Joo. PIFuHD: Multi-level pixel-aligned implicit function for high-resolution 3D human digitization. In *Computer Vision and Pattern Recognition (CVPR)*, pages 84–93, 2020. 2, 3

[73] Nikolaos Sarafianos, Bogdan Boteanu, Bogdan Ionescu, and Ioannis A. Kakadiaris. 3D human pose estimation: A review of the literature and analysis of covariates. *Computer Vision and Image Understanding (CVIU)*, 152:1–20, 2016. 2

[74] Manolis Savva, Angel X Chang, Pat Hanrahan, Matthew Fisher, and Matthias Nießner. PiGraphs: Learning interaction snapshots from observations. *Transactions on Graphics (TOG)*, 35(4):139:1–139:12, 2016. 2, 3, 6, 7, 8

[75] A. Schodl and I. Essa. Depth layers from occlusions. In *Computer Vision and Pattern Recognition (CVPR)*, pages 639–644, 2001. 2

[76] Daeyun Shin, Zhile Ren, Erik B Sudderth, and Charless C Fowlkes. 3D scene reconstruction with multi-layer depth and epipolar transformers. In *International Conference on Computer Vision (ICCV)*, pages 2172–2182, 2019. 3

[77] Vincent Sitzmann, Michael Zollhöfer, and Gordon Wetzstein. Scene representation networks: Continuous 3D-structure-aware neural scene representations. In *Conference on Neural Information Processing Systems (NeurIPS)*, 2019. 3

[78] David Smith, Matthew Loper, Xiaochen Hu, Paris Mavroidis, and Javier Romero. FACSIMILE: Fast and accurate scans from an image in less than a second. In *International Conference on Computer Vision (ICCV)*, pages 5329–5338, 2019. 2

[79] Yu Sun, Wu Liu, Qian Bao, Yili Fu, Tao Mei, and Michael J. Black. Putting people in their place: Monocular regression of 3D people in depth. In *CVPR*, 2022. 1

[80] Omid Taheri, Vassileios Choutas, Michael J. Black, and Dimitrios Tzionas. GOAL: Generating 4D whole-body motion for hand-object grasping. In *Computer Vision and Pattern Recognition (CVPR)*, 2022. 3

[81] Omid Taheri, Nima Ghorbani, Michael J. Black, and Dimitrios Tzionas. GRAB: A dataset of whole-body human grasping of objects. In *European Conference on Computer Vision (ECCV)*, pages 581–600, 2020. 3

[82] Bugra Tekin, Isinsu Katircioglu, Mathieu Salzmann, Vincent Lepetit, and Pascal Fua. Structured prediction of 3D human pose with deep neural networks. In *British Machine Vision Conference (BMVC)*, pages 130.1–130.11, 2016. 2

[83] Denis Tome, Chris Russell, and Lourdes Agapito. Lifting

from the deep: Convolutional 3D pose estimation from a single image. In *Computer Vision and Pattern Recognition (CVPR)*, pages 5689–5698, 2017. 2

[84] Gul Varol, Duygu Ceylan, Bryan Russell, Jimei Yang, Ersin Yumer, Ivan Laptev, and Cordelia Schmid. BodyNet: Volumetric inference of 3D human body shapes. In *European Conference on Computer Vision (ECCV)*, pages 20–38, 2018. 2

[85] Nanyang Wang, Yinda Zhang, Zhuwen Li, Yanwei Fu, Wei Liu, and Yu-Gang Jiang. Pixel2mesh: Generating 3D mesh models from single RGB images. In *ECCV*, pages 52–67, 2018. 3

[86] Philippe Weinzaepfel, Romain Brégier, Hadrien Combaluzier, Vincent Leroy, and Grégory Rogez. DOPE: Distillation of part experts for whole-body 3D pose estimation in the wild. In *European Conference on Computer Vision (ECCV)*, pages 380–397, 2020. 2

[87] Zhenzhen Weng and Serena Yeung. Holistic 3D human and scene mesh estimation from single view images. In *Computer Vision and Pattern Recognition (CVPR)*, pages 334–343, 2021. 1, 2, 3, 5, 6, 7, 8

[88] Donglai Xiang, Hanbyul Joo, and Yaser Sheikh. Monocular total capture: Posing face, body, and hands in the wild. In *Computer Vision and Pattern Recognition (CVPR)*, pages 10957–10966, 2019. 3

[89] Yuliang Xiu, Jinlong Yang, Dimitrios Tzionas, and Michael J. Black. ICON: Implicit Clothed humans Obtained from Normals. In *Computer Vision and Pattern Recognition (CVPR)*, 2022. 2, 3

[90] Hongyi Xu, Eduard Gabriel Bazavan, Andrei Zanfir, William T. Freeman, Rahul Sukthankar, and Cristian Sminchisescu. GHUM & GHUML: Generative 3D human shape and articulated pose models. In *Computer Vision and Pattern Recognition (CVPR)*, pages 6183–6192, 2020. 2

[91] Lixin Yang, Xinyu Zhan, Kailin Li, Wenqiang Xu, Jiefeng Li, and Cewu Lu. CPF: Learning a contact potential field to model the hand-object interaction. In *International Conference on Computer Vision (ICCV)*, pages 11097–11106, 2021. 3

[92] Ye Yuan, Umar Iqbal, Pavlo Molchanov, Kris Kitani, and Jan Kautz. GLAMR: Global occlusion-aware human mesh recovery with dynamic cameras. In *Computer Vision and Pattern Recognition (CVPR)*, 2022. 1

[93] Ye Yuan, Shih-En Wei, Tomas Simon, Kris Kitani, and Jason Saragih. SimPoE: Simulated character control for 3D human pose estimation. In *Computer Vision and Pattern Recognition (CVPR)*, pages 7159–7169, 2021. 1

[94] Andrei Zanfir, Elisabeta Marinoiu, and Cristian Sminchisescu. Monocular 3D pose and shape estimation of multiple people in natural scenes - the importance of multiple scene constraints. In *Computer Vision and Pattern Recognition (CVPR)*, pages 2148–2157, 2018. 3

[95] Cheng Zhang, Zhaopeng Cui, Yinda Zhang, Bing Zeng, Marc Pollefeys, and Shuaicheng Liu. Holistic 3D scene understanding from a single image with implicit representation. In *Computer Vision and Pattern Recognition (CVPR)*, pages 8833–8842, 2021. 1, 3

[96] Jason Y Zhang, Sam Pepose, Hanbyul Joo, Deva Ramanan, Jitendra Malik, and Angjoo Kanazawa. Perceiving 3D human-object spatial arrangements from a single image in the wild. In *European Conference on Computer Vision (ECCV)*, pages 34–51, 2020. 2, 3, 4, 5

[97] Siwei Zhang, Yan Zhang, Federica Bogo, Pollefeys Marc, and Siyu Tang. Learning motion priors for 4D human body capture in 3D scenes. In *International Conference on Computer Vision (ICCV)*, pages 11323–11333, 2021. 8

[98] Siwei Zhang, Yan Zhang, Qianli Ma, Michael J. Black, and Siyu Tang. PLACE: Proximity learning of articulation and contact in 3D environments. In *International Conference on 3D Vision (3DV)*, 2020. 3, 6

[99] Yan Zhang, Mohamed Hassan, Heiko Neumann, Michael J Black, and Siyu Tang. Generating 3D people in scenes without people. In *Computer Vision and Pattern Recognition (CVPR)*, pages 6194–6204, 2020. 3, 6

[100] Yinda Zhang, Shuran Song, Ersin Yumer, Manolis Savva, Joon-Young Lee, Hailin Jin, and Thomas Funkhouser. Physically-based rendering for indoor scene understanding using convolutional neural networks. In *Computer Vision and Pattern Recognition (CVPR)*, pages 5287–5295, 2017. 3

[101] Yibiao Zhao and Song-Chun Zhu. Scene parsing by integrating function, geometry and appearance models. In *Computer Vision and Pattern Recognition (CVPR)*, pages 3119–3126, 2013. 3

[102] Zerong Zheng, Tao Yu, Yixuan Wei, Qionghai Dai, and Yebin Liu. DeepHuman: 3D human reconstruction from a single image. In *International Conference on Computer Vision (ICCV)*, pages 7738–7748, 2019. 2

[103] Michael Zollhöfer, Patrick Stotko, Andreas Görlitz, Christian Theobalt, Matthias Nießner, Reinhard Klein, and Andreas Kolb. State of the art on 3D reconstruction with RGB-D cameras. *Computer Graphics Forum (CGF)*, 37(2):625–652, 2018. 2